

Coarse-grained molecular dynamics modeling of DNA–carbon nanotube complexes

Jian Zou, Wentao Liang and Sulin Zhang^{*,†}

Department of Engineering Science and Mechanics, Pennsylvania State University, University Park, PA 16802, U.S.A.

SUMMARY

We present a coarse-grained method to study the energetics and morphologies of DNA–carbon nanotube (DNA-CNT) complexes in aqueous environment. In this method, we adopt an existing coarse-grained DNA model in which each nucleotide is coarse-grained by two interaction sites, one for the phosphate and sugar groups and the other for the base group. The interaction potentials between DNA sites and the carbon atoms on a CNT are parameterized through all-atom molecular dynamics (MD) simulations. The water molecules are treated implicitly using Langevin dynamics. The coarse-grained DNA-CNT model significantly improves the computational affordability, while captures the essential dynamics of DNA-CNT interactions observed from all-atom MD simulations. The coarse-grained method enables us to efficiently simulate adhesion, encapsulation, and wrapping processes of a single-stranded DNA molecule around CNTs. The simulation results agree with those obtained by all-atom MD simulations in several aspects. Our coarse-grained simulations provide useful guidelines in positioning DNA molecules on a CNT surface or graphene substrate in single-molecule experimental studies. Copyright © 2009 John Wiley & Sons, Ltd.

Received 26 July 2009; Revised 26 October 2009; Accepted 9 November 2009

KEY WORDS: molecular dynamics; multi-scale modeling; coarse-grained simulations; DNA; carbon nanotubes

1. INTRODUCTION

Interfacing biological molecules with carbon nanotubes (CNTs) has become significant interest in recent years because of the great potentials of developing biocompatible systems, bioelectronic sensors, and tissue scaffolds for the culture and growth of biological cells. One particular interesting example is the attachment of single-stranded DNA (ssDNA) onto CNTs to form DNA-CNT hybrids

*Correspondence to: Sulin Zhang, Department of Engineering Science and Mechanics, Pennsylvania State University, University Park, PA 16802, U.S.A.

†E-mail: suz10@psu.edu

Contract/grant sponsor: National Science Foundation (NSF); contract/grant numbers: 0600661(0826841), 0600642

[1, 2]. It has been shown that ssDNA can be wrapped onto a CNT surface through π -stacking, or covalently linked onto the CNT sidewall or end tips through surface-bonded carboxylic groups, or encapsulated into the hollow interior of CNTs [3–6]. The DNA-functionalized CNTs result in effective dispersion of CNT bundles in aqueous solution, which has enabled many applications [4]. The immobilization of DNA molecules modifies the electro-mechanical properties of the otherwise intact CNTs, forming the basis of single-molecule biological sensors of CNTs. The ssDNA-CNT hybrid, benefiting from both the unique physical properties of CNTs and the specific molecular recognition capabilities of the immobilized ssDNA, represents a unique anchoring platform capable of assembling a wide range of materials, and holds great promise for potential applications in biochemical sensing, protein immobilization, drug delivery, DNA transfection, and gene sequencing [3–5, 7–9]. For example, the immobilized ssDNA can further hybridize with the complementary DNA strands to form double-stranded DNA (dsDNA) [10]. A fundamental understanding is crucial to the realization and regulation of these applications of the DNA-CNT hybrids.

Both DNAs and CNTs have attracted intensive research interests since their discoveries. The standard building blocks for DNA molecules are nucleotides, which have three characteristic components: a phosphate, a sugar group (deoxy-ribose), and a nitrogenous base [10]. An ssDNA molecule is a linear polymer composed of the sugar-phosphate backbone to which four different bases, adenine (ADE or A), guanine (GUA or G), cytosine (CYT or C), and thymine (THY or T), are covalently bonded. The base sequence encodes the entire genetic information in living cells. The famous double helical structure of B-DNA, discovered by Watson and Crick [1], consists of two complementary strands that run in opposite directions and wind around each other, and are joined by hydrogen bonds between complementary bases, A-T and C-G. The complementary base-pairing gives rise to informational redundancy and allows for chemical fidelity in replication. CNTs are one-dimensional macromolecules consisting of single or multiple graphene sheets rolled into a cylindrical configuration [11]. According to the number of graphene layers, CNTs can be single-walled (SWCNTs) or multi-walled (MWCNTs), and can have a very large aspect ratio with a diameter of several nanometers and length up to tens of microns. CNTs are light-weight, ultra-stiff, and have extremely high surface-to-volume ratios, making them ideal mechanical reinforcements in high-performance composites and platforms for protein immobilization. CNTs also have excellent thermal and electrical conductivities, thus are good candidates for sensors [12–14] and nano-electronic devices [15].

Numerous methods have been adopted to study the materials properties of DNAs and CNTs, ranging from quantum mechanical (QM) simulations, all-atom molecular dynamics (MD) simulations, to continuum mechanics. Separate reviews on the studies of DNAs and CNTs are beyond the scope of this article; the readers may refer to several review articles for the current status of these studies (e.g. [16, 17]). Instead, we will focus on the recent advances in the coarse-grained simulations of DNAs and CNTs and all-atom MD simulations of DNA-CNT complexes. For microscopic understanding with atomic-level details, all-atom MD simulations with empirical force fields have been widely adopted to elucidate the DNA-CNT interfaces. Gao *et al.* [5] reported that a DNA molecule can be spontaneously inserted into CNTs in aqueous environment, where the van der Waals (vdW) and hydrophobic forces are important for the insertion process, with the former playing a dominant role. They also found that the insertion kinetics is strongly dependent on the tube sizes [5, 18]. Zheng *et al.* [4] found that an ssDNA may exhibit a variety of configurations when interacting with a CNT; helical wrapping and linear adsorption are two of the possible configurations. Johnson *et al.* [6] also studied the self-assembling mechanisms, structure, and energetics of ssDNA-CNT complexes. They observed that SWCNT induces ssDNA to undergo a

spontaneous conformational change that enables self-assembly of the complexes via the π -stacking between DNA bases and the sidewall of SWCNTs. The self-assembled complex features right- or left-handed helical wrapping of ssDNA on the SWCNT sidewalls.

Though all-atom MD simulations have provided insights into the DNA-CNT interactions, the computational costs have limited such studies to a relatively small system typically involving a few hundred thousand atoms and to a time scale on the order of nanoseconds [5, 6, 19]. On the other end of length scale spectrum, overly simplified continuum theories [20, 21] failed to include the important atomistic details of DNA-CNT interactions. As a result, a tremendous gap between experiments and modeling exists, which has motivated a continual search for coarse-grained methods [19, 22–29] that bridge simulations and experiments. Coarse-grained models for DNA molecules and CNTs have both been developed in the last decade, whereas the coarse-graining schemes are markedly different. A CNT is a highly symmetric molecule for which a representative unit consists of only two inequivalent nuclei and three inequivalent bonds. The coarse-graining description involves homogenization of the discrete representation of the short-range covalent binding energy and the long-range vdW energy. Based on the Cauchy-Born rule, the deformed lattice vectors and the angles between the lattice vectors can be analytically expressed via the continuum measures [25–27, 30]. A hyperelastic strain-energy density function can be then cast from the interatomic potentials within the framework of finite crystal elasticity. The energy density functions then serve as the constitutive relations for the continuum, with which the CNT is coarse-grained by finite elements. Since the interatomic potential is analytically embedded into the coarse-scale energy density functions, this coarse-graining scheme significantly improves the computational affordability, while remaining faithful to the nonlinearity of the interatomic potentials. Unlike the coarse-graining scheme for CNTs in which the atomic interaction energies are first homogenized into continuum constitutive relations, followed by the partition of the system into coarse grains (finite element nodes), the coarse-grained models for DNA molecules [19, 22–24] are established by first grouping a cluster of atoms into a single coarse-grained particle, followed by the construction of an equivalent inter-particle interaction potential. The complexity of such coarse-grained approaches varies in their level of details, depending on the number of particles per nucleotide. The model of Huertas *et al.* [22] simply represents each nucleotide by one bead, where the beads are connected by harmonic springs. The model of Drukker and Schatz [19] simplifies each nucleotide into two particles, i.e., a backbone site and a base site. The model has successfully simulated the hybridization of complementary ssDNA and denaturation of dsDNA at elevated temperatures. Tepper and Voth [24] developed a coarse-grained dsDNA model, where the base pairs are represented by co-planar, connected particles, and two identical particles are used to represent the backbone per base pair. This model successfully simulated the spontaneous assembly of a linear initial configuration into a double helix. The coarse-grained model developed by Knotts *et al.* [23] reduces each nucleotide into three interaction sites, one each for the phosphate, sugar, and base. A major improvement of this model as compared to the model of Drukker and Schatz is that it includes the Columbic interactions. This model was able to predict several aspects of DNA behavior, including salt-dependent melting, bubble formation and rehybridization, and the mechanical properties of the molecule as a function of salt concentration. For all the coarse-grained models, the inter-particle interaction potentials are parameterized by matching a set of thermodynamic properties of DNAs obtained either from literature and experiments, or classical MD simulations.

Despite the advance in the coarse-grained modeling of DNA molecules, such coarse-grained models have not been exploited to study DNA-CNT interactions. In this article, we develop a

coarse-grained model for DNA-CNT complexes by coupling an existing coarse-grained DNA model with atomistic CNT model. The morphologies and energetics of several different DNA-CNT assemblies are studied using this coarse-grained model in conjunction with Langevin dynamics. The coarse-grained model is computationally efficient for large-scale simulations, yet sufficiently detailed to capture the essential dynamics of DNA-CNT complexes at atomic scale. Our simulations show that the dynamic evolution and the equilibrium configurations of DNA-CNT complexes depend not only on the size of the CNTs but also on the initial configurations and relative positions of these two molecules. Our coarse-grained modeling results agree quantitatively with existing all-atom calculations in several aspects, which validates the coarse-grained model.

The rest of the paper is organized as follows. We first introduce the coarse-grained DNA model, followed by parameterization of the nonbonding interaction potentials between DNA bases and backbone sites with carbon atoms on CNTs through all-atom MD simulations. The morphologies and energetics of several different DNA-CNT assemblies are then investigated using the coarse-grained model. Finally, we conclude our findings and comment on the coarse-grained method.

2. COARSE-GRAINED MODEL FOR DNA-CNT COMPLEXES

2.1. Coarse-grained DNA model

We will couple the coarse-grained DNA model of Drukker and Schatz [19] with the atomistic CNT model to simulate DNA-CNT interactions. We adopt this particular coarse-grained DNA model for its relative simplicity as compared to the other models. However, one notes that the DNA-CNT coupling strategy presented here is also applicable to other coarse-grained DNA models. For the completeness of our presentation, we give below a brief introduction of the model of Drukker and Schatz [19]. In this coarse-grained DNA model [19], each nucleotide is represented by two interaction sites: a backbone site (representing the sugar ring and the phosphate group) and a base site (representing one of the four DNA bases ADE, THY, CYT, and GUA). As shown in Figure 1, the backbone sites are connected by bonds and each individual base is bonded to its corresponding backbone site. To further stabilize the helical structure, the next-nearest neighbors between the backbone sites are also connected by bonds to increase the stiffness of DNA duplex, which mimics the long-range electrostatic interactions along the negatively charged backbone [19].

The total potential energy for the coarse-grained DNA model includes harmonic bond stretching, cosine angle bending and one-fold dihedral torsion along backbone, a Lennard-Jones (LJ) potential for vdW interactions, and hydrogen bonding (HB) interactions [19]. The total potential energy can be written as:

$$V(r_{ij}, \theta_{ijk}, \phi_{ijkl}) = \frac{1}{2}k_r(r_{ij}-r_0)^2 + \frac{1}{2}k_\theta(\cos\theta_{ijk}-\cos\theta_0)^2 + \frac{1}{2}K_\phi(1-\cos(\phi_{ijkl}-\phi_0)) + 4\varepsilon_{ij} \left[\left(\frac{\sigma_{ij}}{r_{ij}}\right)^{12} - \left(\frac{\sigma_{ij}}{r_{ij}}\right)^6 \right] + V_{HB}(r; \phi), \quad (1)$$

where r_{ij} denotes the distance between two interaction sites; θ_{ijk} and ϕ_{ijkl} are the bending and torsional angles; r_0 , θ_0 , and ϕ_0 are the equilibrium values for bond length, the bending and torsion angles determined from the DNA double-helical structure, respectively; σ_{ij} and ε_{ij} are the LJ parameters; the k_r , k_θ , and k_ϕ are the corresponding force constants. The HB interaction potential

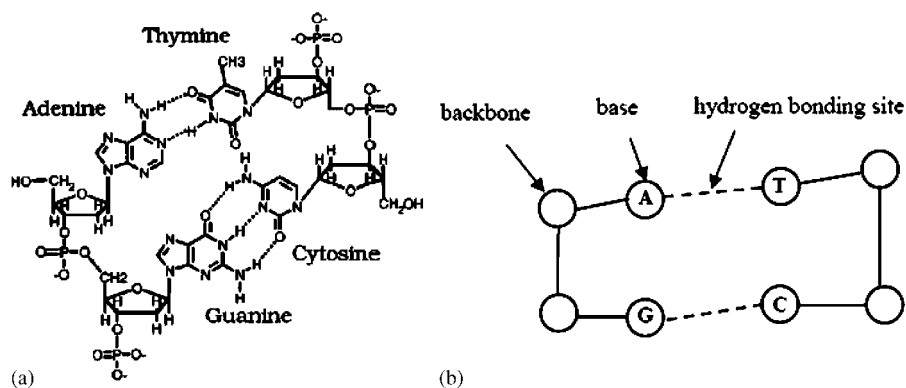


Figure 1. The coarse-grained DNA model reduces each nucleotide into two interaction sites: a backbone site (representing the sugar ring and the phosphate group) and a base site [11]; complementary bases are paired through hydrogen bonding interactions: (a) all-atom representation and (b) coarse-grained description.

depends on both the donor–acceptor distance r and the angle ϕ between backbone, donor, and acceptor with the following form [19]:

$$V_{\text{HB}} = (V_{\text{H1}}(r) - V_{\text{H2}}(r)) \cdot f(\phi); \quad (2a)$$

$$V_{\text{H1}} = v_0(\exp[-\alpha(r - r_{\text{H}}^{\text{eq}})] - 1)^2 - v_0; \quad (2b)$$

$$V_{\text{H2}} = \frac{1}{4}v_0(\tan h[\beta(r - r_{\text{H}}^*)] - 1); \quad (2c)$$

$$f(\phi) = \frac{1}{2}(\cos(\gamma\phi) + 1) \quad \phi_{\text{min}} \leq \phi \leq \phi_{\text{max}} \quad (2d)$$

$$= 0 \quad \text{otherwise,} \quad (2e)$$

where the first part V_{H1} describes the donor–acceptor interactions, and the second part V_{H2} mimics the solvent effect, and $f(\phi)$ is an angle-dependent term, which restricts the angle ϕ in a certain range and is otherwise zero, v_0 , α , β , γ , r_{H}^{eq} , and r_{H}^* are the corresponding parameters. Each base may have several hydrogen bonding sites: in A–T base pair, the base ADE has one donor site and one acceptor site that match up with the acceptor and donor sites on THY, respectively; while in C–G base pair, the base CYT has one donor site and two acceptor sites corresponding to one acceptor and two donor sites on base GUA, respectively. Other base pairs are considered as mismatch in our simulations and the HB interactions between them are taken to be zero instead of using the mixing rules. HB interaction between bases on the same strand is also included, which is necessary to simulate the formation of loop structures for very long self-complementary DNA strands.

All the parameters for the coarse-grained DNA model can be found in Reference [18]. It is worth noting that the coarse-grained DNA model is constructed to give a reasonable melting behavior only at a specific salt concentration of $\sim 0.1\text{M}$ [19], which is commonly used in experiments.

2.2. Interaction potential between DNA sites and a single carbon atom on CNT surface

To facilitate simulations of DNA-CNT interactions, the interaction potentials between the coarse-grained DNA sites and the carbon atoms need to be established. Note that we did not coarse-grain the CNT since the effective radii of the DNA interaction sites indicated from their LJ parameters are comparable to that of a carbon atom. To simplify our analysis, we choose the classical 12-6 LJ potential to describe the interactions between the DNA sites and carbon atoms:

$$V_{\text{SC}}(r) = 4\varepsilon_{\text{SC}} \left[\left(\frac{\sigma_{\text{SC}}}{r} \right)^{12} - \left(\frac{\sigma_{\text{SC}}}{r} \right)^6 \right] \quad (3)$$

where ε_{SC} and σ_{SC} are the two LJ parameters, and r is the distance between the center-of-mass of the DNA interaction sites and the carbon atoms on the CNT surface. The total vdW interaction energy between the site and the carbon atom is the discrete sum of the LJ potential energy. Homogenizing the discrete interaction energy gives rise to the vdW interaction energy density [27], as

$$w_{\text{SC}}(r) = \frac{2}{S_0} V_{\text{SC}}(r) \quad (4)$$

where S_0 is the unit cell of the CNT surface, containing two unique nuclei (thus a factor of 2 appears). The total vdW interaction energy $E_{\text{S-CNT}}$ between the site and the CNT surface can be then analytically expressed as an integral over the CNT surface [27]:

$$E_{\text{S-CNT}}(\varepsilon_{\text{SC}}; \sigma_{\text{SC}}) = \int_{\Omega} w_{\text{SC}}[\|\mathbf{q}_0 - \mathbf{x}\|] d\Omega \quad (5)$$

where \mathbf{q}_0 is the location of the center of the mass of the DNA interaction site, \mathbf{x} is a material point on the CNT surface Ω . Note that after the analytical integration, the total vdW interaction energy is a function of the two LJ parameters, ε_{SC} and σ_{SC} . Note that the equilibrium distance $r_{\text{S-CNT}}^{\text{eq}}$ between the interaction sites only depends on σ_{SC} . These two LJ parameters are then determined from all-atom MD simulations, as described below.

In our all-atom MD simulations, DNA molecules are modeled by the empirical AMBER99 force field [31] with sodium counterions included to neutralize the entire system. The carbon atoms on CNTs are uncharged and the corresponding carbon-carbon interaction is described by a Morse potential for bond stretching, a harmonic cosine potential for angle bending, a 2-fold cosine potential for dihedral torsion, and a LJ potential for non-bonding interactions [32]:

$$V(r_{ij}, \theta_{ijk}, \phi_{ijkl}) = K_{Cr} [\exp(-\gamma(r_{ij} - r_C)) - 1]^2 + \frac{1}{2} K_{C\theta} (\cos \theta_{ijk} - \cos \theta_C)^2 + \frac{1}{2} K_{C\phi} (1 + \cos(2\phi_{ijkl} - \phi_C)) + 4\varepsilon_{\text{CC}} \left[\left(\frac{\sigma_{\text{CC}}}{r_{ij}} \right)^{12} - \left(\frac{\sigma_{\text{CC}}}{r_{ij}} \right)^6 \right], \quad (6)$$

where r_C , θ_C , and ϕ_C are the reference geometrical parameters for CNT; K_{Cr} , $K_{C\theta}$, and $K_{C\phi}$ are the force constants of stretching, bending, and torsion, respectively; ε_{CC} and σ_{CC} are the carbon-carbon LJ parameters. The water solvent is described by the empirical transferable intermolecular potential 3 point (TIP3P) model [33], which effectively accounts for intra-molecular degrees of freedom including the harmonic O-H bond stretching and H-O-H angle bending, as

$$V(r_{ij}, \theta_{ijk}) = \frac{1}{2} K_{Wr} (r_{ij} - r_W)^2 + \frac{1}{2} K_{W\theta} (\cos \theta_{ijk} - \cos \theta_W)^2, \quad (7)$$

Table I. LJ parameters between backbone and base sites in the coarse-grained DNA and the carbon atoms on CNTs extracted from all-atom MD simulations.

Interaction sites	σ (nm)	ε (kJ mol ⁻¹)
ADE	0.3357	4.8250
GUA	0.3421	5.0455
CYT	0.3385	3.8306
THY	0.3411	4.2709
Backbone	0.4067	2.7494

where r_W and θ_W denote the reference O-H bond length and H-O-H angle, respectively; K_{Wr} and $K_{W\theta}$ are the corresponding force constants. The non-bonding interactions between water molecules include an oxygen–oxygen LJ potential and an electrostatic potential between point charges on oxygen and hydrogen atoms. The CNT–water interaction is modeled by a carbon–oxygen LJ potential.

All-atom MD simulations of DNA-CNT systems in a water solution are performed using the MD package GROMACS [34, 35] at room temperature of 300 K (unless otherwise specified) and atmospheric pressure of 1 bar [36], with a time step of 1 fs (1 fs = 10⁻¹⁵ s), and periodic boundary conditions applied in three orthogonal directions. The electrostatic interactions are evaluated using the particle mesh Ewald (PME) method with cubic-spline interpolation and 0.1 nm grid width [37]. The all-atom MD simulations give rise to the vdW energy E_{S-CNT} and the equilibrium distance r_{S-CNT}^{eq} between the center-of-mass of the DNA interaction sites and the CNT surface from which the two LJ parameters in Equation (3) can be determined, as listed in Table I. Our coarse-grained simulations described in the succeeding sections show that the fitted LJ potential describes the DNA-CNT interactions well.

2.3. Coarse-grained simulations of DNA-CNT interactions

To further simplify the calculations, the solvent effect is treated implicitly by stochastic frictional forces using Langevin dynamics. The friction constant ζ associated with the bath is related to the solvent viscosity η by [19]:

$$\zeta = \frac{4\pi}{m} \eta \cdot r_{\text{eff}}, \quad (8)$$

where $r_{\text{eff}} = 0.5$ nm is the solute's effective hydrodynamic radius and m is the mass of coarse-grained particles. The temperature-dependent viscosity η for water is calculated using the following empirical equations [19]

$$\eta = \eta_{20} \cdot \exp(-A/B); \quad (9a)$$

$$A = 1.37023(T - 20) + 8.36 \times 10^{-4}(T - 20)^2; \quad (9b)$$

$$B = 109 + T, \quad (9c)$$

where T is the temperature, $\eta_{20} = 0.93975 \times 10^{-3} \text{ kg m}^{-1} \text{ s}^{-1}$ is the viscosity at 20°C for water. The use of Equations (8) and (9) results in a value of ζ in the range of 10–30 ps⁻¹ (1 ps = 10⁻¹² s) for $T = 0$ –100°C.

With these treatments, the coarse-grained model reduces dramatically the number of degrees of freedom by several orders of magnitude. In addition, the coarse-graining suppresses the high-frequency vibration of light atoms such as hydrogen atoms in DNA and water molecules. Thus, a much larger time step (~ 10 fs) can be used to simulate a much larger system in the microsecond time scale, which is inaccessible to all-atom MD simulations.

3. RESULTS AND DISCUSSION

3.1. Adhesion of DNA to CNT surface

The adhesion energies between four DNA bases and single-walled CNTs (SWCNTs) with different radii are calculated using the coarse-grained model described in the previous section. The results are compared with those of all-atom MD simulations to validate the model. Since SWCNTs can be viewed as a cylindrical shell, of which the adhesion energy to its exterior and interior surface should exhibit different strength due to the curvature effect, two sets of simulations are performed with the DNA bases placed initially outside and inside the SWCNTs, respectively. Each simulation is carried out for at least 10 ns to ensure that the DNA strand has fully adhered to the CNT sidewall and the system has reached equilibrium. Additional simulation of 40 ns is performed for data collection and analysis.

The adhesion between the four DNA bases at the exterior surface of a (6,6) SWCNT is first studied as a representative study. Note that each of the two purine bases ADE and GUA contains two aromatic rings, while each of the two pyrimidine bases CYT and THY has only one aromatic ring. The difference in the chemical structures explains that the purine bases have a relatively higher adhesion energies (60.66 and $65.40 \text{ kJ mol}^{-1}$ for bases ADE and GUA, respectively) than the pyrimidine bases (47.87 and $53.81 \text{ kJ mol}^{-1}$ for bases CYT and THY, respectively). Standard error of the adhesion energies for the four bases falls in the range of $2.7\text{--}2.8 \text{ kJ mol}^{-1}$. After attaching to the SWCNT, the DNA strand is held tightly against the tube wall in the radial direction, yet able to move nearly freely along the axial and circumferential directions under thermal fluctuations. It is found that base CYT is most mobile on the tube surface because of its smallest weight among the four bases. Considering the much simpler model used here, these adhesion energies as well as the trend ($\text{GUA} > \text{ADE} > \text{THY} > \text{CYT}$) agree very well with all-atom calculations (57.84 , 62.66 , 46.28 , and $53.02 \text{ kJ mol}^{-1}$ for ADE, GUA, CYT, and TYT on a SWCNT of similar radius, respectively [6]) and experimental measurements [38–41].

Figure 2 shows that the DNA-CNT adhesion energy increases for the backbone and all the four bases as the tube radius increases when adhesion occurs at the exterior surface of the CNT. The equilibrium distances from the four bases to the tube surface are nearly the same. Thus, the adhesion energy increase is primarily due to the increase in the contact area. When the tube radius approaches infinity, the adhesion energy reaches its value of DNA bases on a planar graphene sheet (77.65 , 84.29 , 62.34 , and $70.77 \text{ kJ mol}^{-1}$ for ADE, GUA, CYT, and THY, respectively). When adhesion occurs at the interior surface of the CNT, the adhesion energy decreases with increasing tube radius, and approaches asymptotically the corresponding value of DNA on a planar graphene when the tube radius is sufficiently large. If one defines a positive tube curvature for exterior adhesion and a negative curvature for the interior adhesion, a uniform trend can be identified: the adhesion energy decreases as the tube curvature increases, which results from the decrease in contact area.

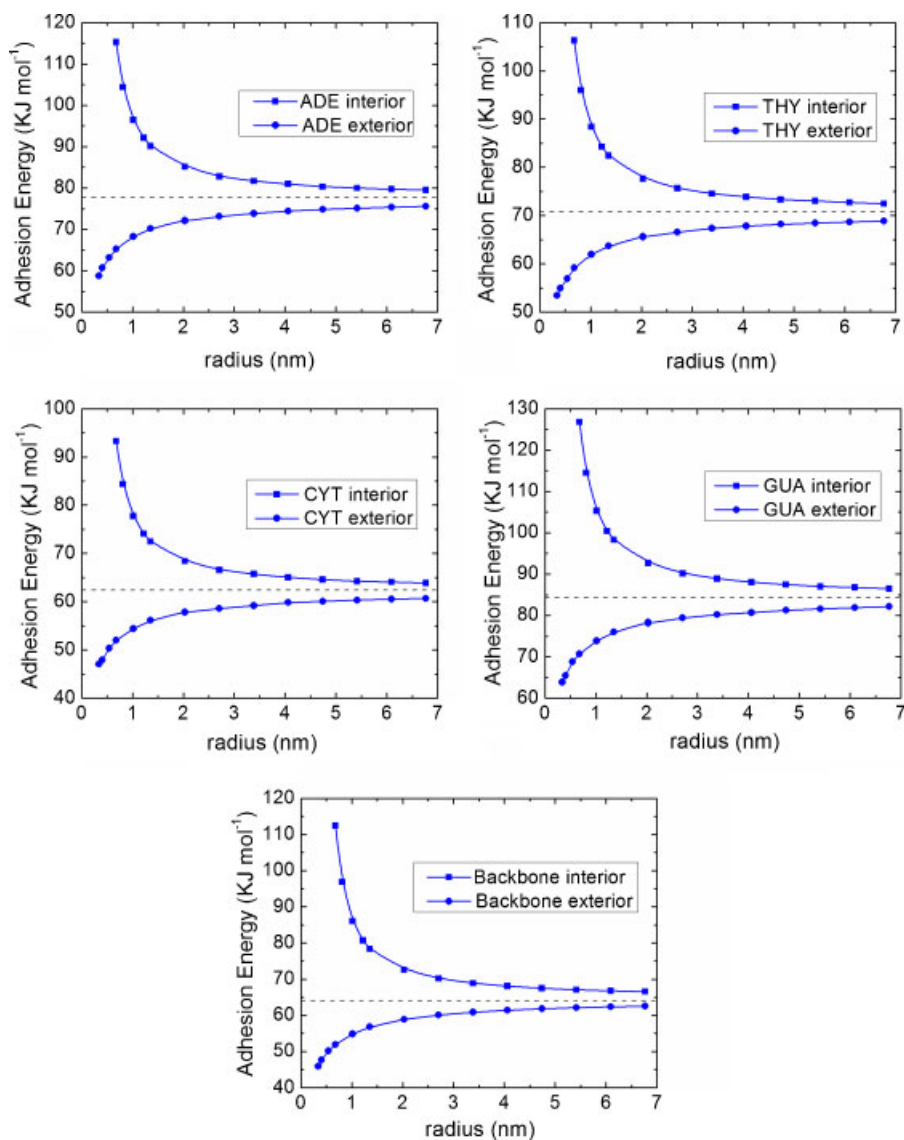


Figure 2. Adhesion energies of the four DNA bases and the backbone with the exterior and interior surfaces of SWCNTs calculated by the coarse-grained simulations.

3.2. Encapsulation of DNA strand into CNT

We next simulate encapsulation of an ssDNA with eight ADE bases into a (10, 10) CNT using the coarse-grained model at room temperature of 300 K. The ssDNA strand is initially placed along the CNT axis. The axial distance between their nearest ends of the CNT and DNA molecule is set to be 0.2 nm, as shown in Figure 3(a). This initial configuration is nearly identical to the setup used in the previous all-atom MD model [5], except that the tube length (~ 5.9 nm) is doubled

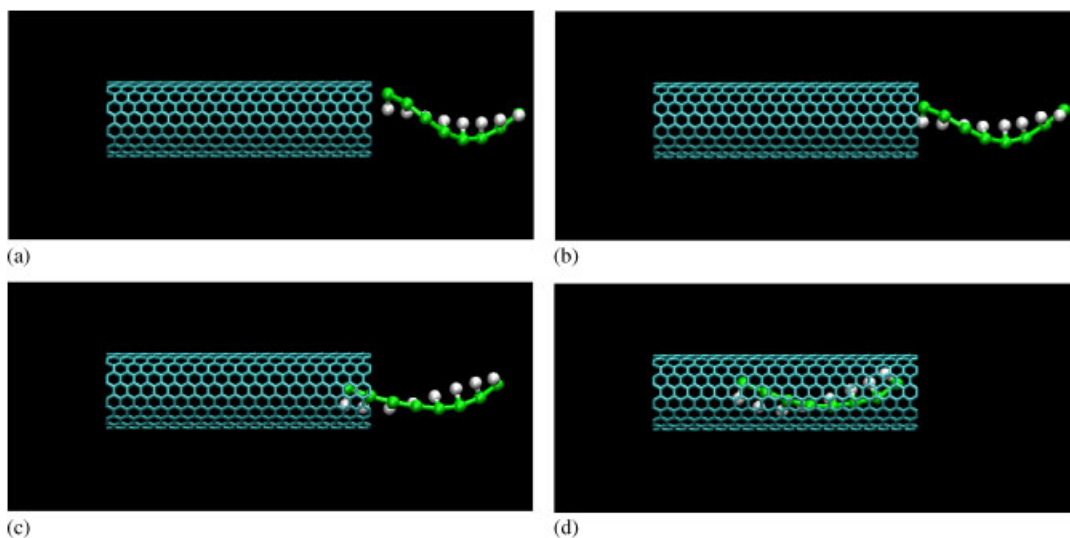


Figure 3. (Color Online) Simulation snapshots (a)–(d) of the encapsulation process of an ssDNA with eight ADE bases into the CNT (10, 10) at $t=0$, 30, 100, and 500 ps, respectively. The tube length is 5.9 nm. The backbone sites are colored in green and the base sites in white.

as compared to that in the all-atom MD simulations to facilitate full encapsulation of the DNA molecule.

The simulation snapshots shown in Figure 3 indicate a very fast insertion process of the ssDNA strand into the CNT. Similar to the predictions of the all-atom MD simulations, the proximal ‘head’ of the ssDNA strand starts to enter the CNT at $t=30$ ps, and the first two bases are fully inside the nanotube at $t=100$ ps. The full encapsulation process is completed at about $t=500$ ps with all the DNA bases inside the tube. The time-scale of the encapsulation process agrees with the all-atom MD results [5]. The self-assembled DNA-CNT system through encapsulation reaches equilibrium afterwards.

The fast encapsulation process can also be viewed from the plot of center-of-mass distance between DNA and CNT as a function of simulation time and the energy evolution of the DNA-CNT vdW interactions (the red and blue curves in Figure 4, respectively). Both the DNA-CNT distance and the DNA-CNT vdW energy continue to decrease at the first 500 ps and thereafter remain nearly constant, indicating that the whole system is equilibrated. The time evolution of the center-of-mass distance appears to agree with the all-atom MD data. It is also observed from the simulation snapshots that the ssDNA strand rotates around the backbone during the encapsulation to unstack from the neighbors, thus enabling each individual base and backbone site to fully adsorb to the CNT surface. Therefore, the encapsulation process is mainly driven by the DNA-CNT nonbonding interactions, penalized by the backbone bending and torsion.

We also examined the temperature effect on the encapsulation process. As shown in Figure 5, the increased simulation temperature can speed up the insertion speed nearly linearly due to the increased molecular mobility, the reduced water viscosity and friction constant (see Equations (8) and (9)). The insertion speed at 400 K is 14.27 nm ns^{-1} , which is comparable to the insertion speed of $\sim 12 \text{ nm ns}^{-1}$ obtained from the all-atom MD simulations [5].

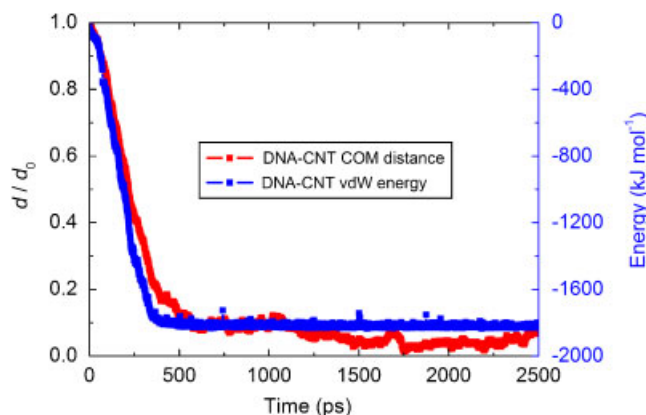


Figure 4. (Color Online) Dynamic process of an ssDNA strand with eight ADE bases encapsulated into a (10, 10) CNT. The red curve is the normalized center-of-mass distance between the DNA and CNT as a function of simulation time, where d_0 is the initial spacing between them. The blue curve is the corresponding evolution of the vdW energy for DNA-CNT interactions. Isolated points indicate the local rotation of backbone of the ssDNA strand.

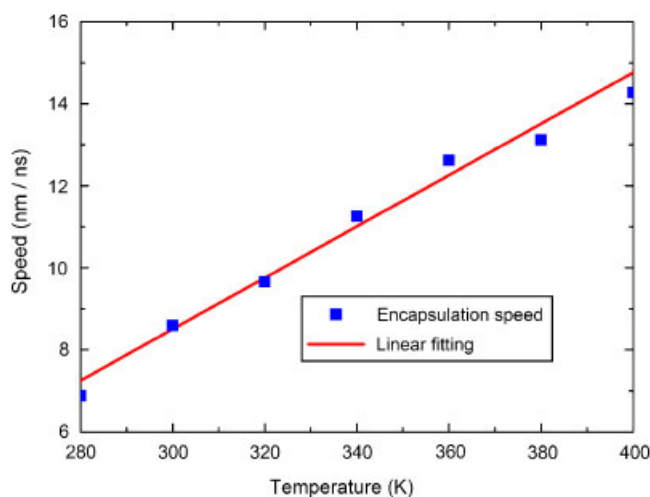


Figure 5. (Color Online) Encapsulation speed of an ssDNA strand with eight ADE bases into a (10, 10) CNT as a function of the simulation temperature. The insertion speed increases nearly linearly with the temperature.

When a single-strand DNA with 20 ADE bases is initially placed vertically to the axis of a (10, 10) tube with the central part facing the entrance as shown in Figure 6(a), it is found that after 10 ns the DNA strand only wraps around the tube end, but does not go inside (Figure 6(b)). This behavior may be attributed to the steric repulsion of the central strand inside the (10, 10) tube (if it is inside the (10, 10) tube, the central part of the tube would feel the steric repulsion from both the nanotube and itself due to the limited space inside the CNT). This explanation is confirmed

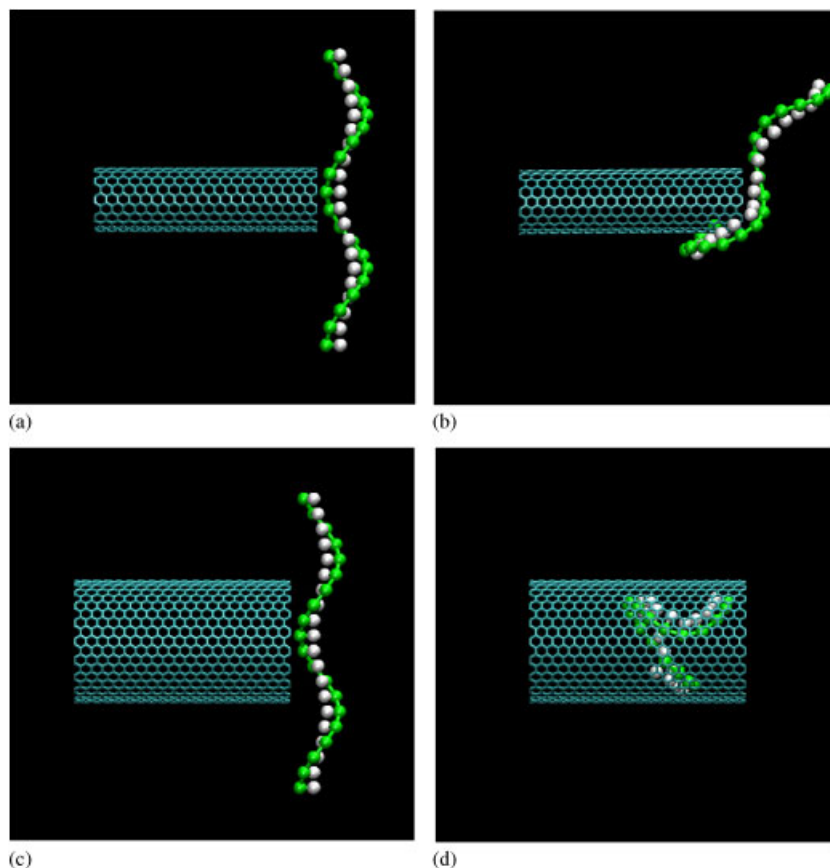


Figure 6. (Color Online) The dependence of the tube radius and initial configuration of a DNA molecule with 20 ADE bases in the encapsulation process. The ssDNA is initially placed perpendicular to the CNT axis. The backbone sites are colored in green and base sites in white. (a), (b) Simulation snapshots for the DNA strand interacting with a (10, 10) CNT at $t=0$ and 10 ns respectively; (c), (d) snapshots for the DNA strand interacting with a (20, 20) CNT at $t=0$ and 10 ns respectively. The DNA strand can be encapsulated into the larger (20, 20) tube, but only wraps around the entrance of the (10,10) tube without going inside.

by replacing the (10,10) tube with (20,20) tube and repeating the simulation (Figure 6(c)). Now there is enough space for the central part to go inside first and the whole DNA strand is successfully encapsulated after 10 ns (Figure 6(d)). During this process, self-contacting loop structure is formed via hydrogen-bonding. However, since only a few hydrogen bonds are formed and the corresponding energy is less than 1 kJ mol^{-1} during most of simulation time, the loop structure is unstable and easy to unloop under thermal fluctuations.

3.3. DNA wrapping around CNT

DNA molecules can also wrap around CNT surface. To study the stability of helical wrapping of DNA outside CNTs, we perform simulations of a (6, 6) CNT wrapped by a single-strand

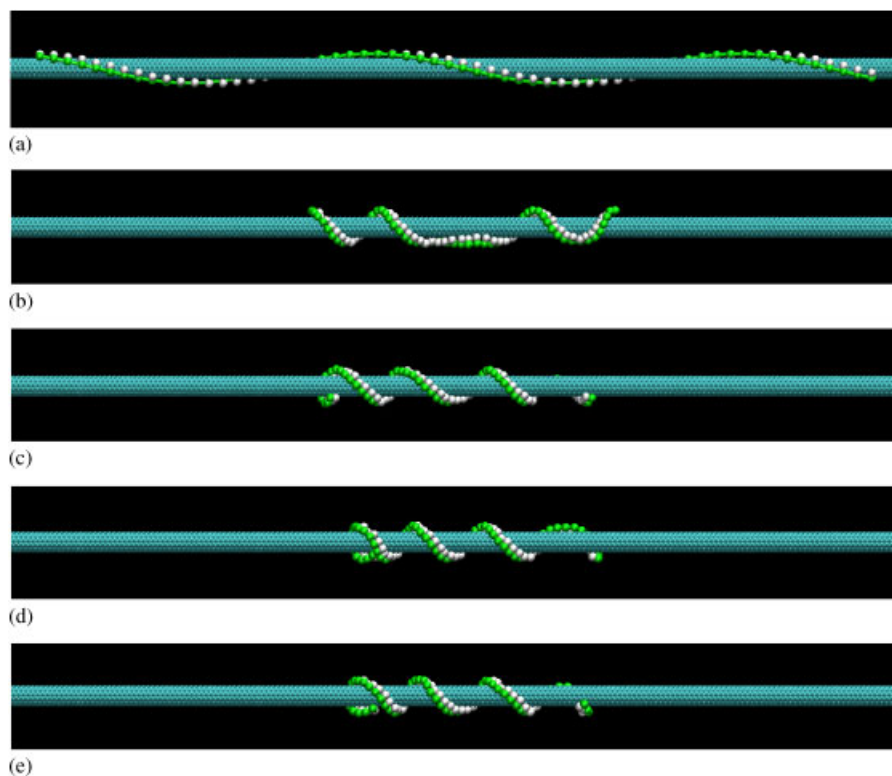


Figure 7. (Color Online) Simulation snapshots of a 60-base-long ssDNA wrapping around a (6,6) CNT with an initial helical pitch of 18 nm. (a)–(e) Configurations at $t=0$, 10, 20, 100, and 200 ns respectively, indicating the formation of a more compact helical wrapping configuration of the DNA strand around the (6,6) tube. The backbone sites are colored in green and base sites in white.

60-base-long poly (GT) sequence with the coarse-grained model. The DNA strand initially adopts a helical pitch of 18 nm and 26 bases per helical turn (Figure 7(a)), which is similar to the setup used in all-atom MD simulations [6]. Figure 7 shows that throughout the simulation, the ssDNA strand maintains the helical structure around the (6,6) CNT, but undergoes an overall reduction in the helical pitch and the end-to-end distance. Upon reaching the equilibrium (after 100 ns), the pitch value is 3.3 ± 0.3 nm and the number of bases per helical turn is about 15. The pitch value falls in the range of all-atom MD simulations (2–8 nm) [6].

Further energetic analysis shows that although the initial helical configuration of DNA tends to minimize the steric repulsion and bond stretching [6], the backbone is still bent and twisted. Since the DNA strand is already very close to the tube wall in the radial direction, the DNA-CNT vdW energy reduction during the helical condensation is relatively small (about 500 kJ mol^{-1} , see blue curve in Figure 8). Instead, because the energy barrier for the bases and backbone sites to move along the axial and circumferential directions at the CNT surface is very low, the DNA strand tends to unwind its backbone to release the strain energy stored in its bent and twisted backbone (see red curve in Figure 8). This drives the formation of an energetically more favorable and more compact helical structure. In addition, the unwound configuration could also

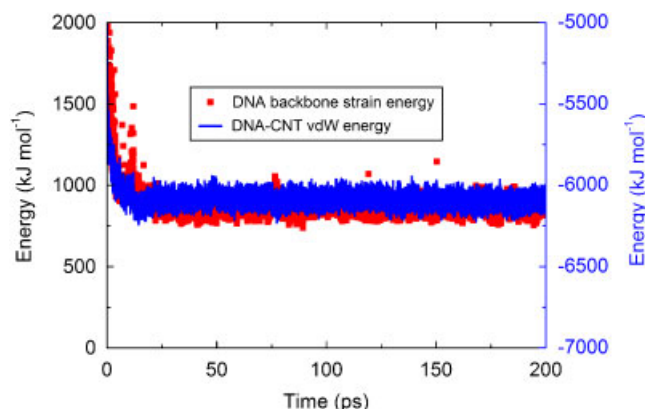


Figure 8. (Color Online) Energy evolution during the helical condensation process of a 60-base-long ssDNA wrapping around a (6,6) CNT with an initial helical pitch of 18 nm. The evolution of the DNA backbone strain energy is shown by the red curve, while that of the DNA-CNT vdW energy shown in blue curve.

increase the contact area between the DNA strand at the CNT sidewall and thus result in a further reduction in the DNA-CNT vdW interaction energy. Therefore, although the DNA-CNT self-assembling process is mainly driven by the DNA-CNT vdW interactions, the final wrapping configuration of the DNA strand near the tube wall should be the result from the interplay between the DNA-CNT nonbonding interactions and the bonding interaction from the backbone bending and torsion.

The same ssDNA molecule and CNT are used to study the effects of the initial configurations on the final wrapping structures, as shown in Figure 9. The ssDNA initially takes a linear configuration, and forms an angle of ϑ with the CNT axis. Coarse-grained simulations were performed sufficiently long to ensure that equilibrium was reached. Different wrapping structures, including helices, looping, U-shaped, disordered, and self-contacting wrapping structures or the combinations, were obtained, depending on the angle ϑ set in the initial configurations. In contrast to the diverse wrapping structures, the equilibrium potential energies of these configurations are comparable, indicating that there might be several possible mechanisms for DNA wrapping around CNTs. Similar diverse wrapping structures were also reported in all-atom MD simulations [6].

We further simulated DNA wrapping inside CNTs, where the CNTs act as a cylindrical confinement for the DNA strand. The same DNA strand (shown in Figure 9) was used and initially placed in the center of the tube with a helical structure. Our simulations show that the initial helical structure is maintained for small tubes (CNTs (10, 10) and (12, 12)) and the helical pitch decreases as the tube radius increases, as shown in Figure 10. For larger tubes, the helical structure can be no longer maintained and random chiral, U-shaped, and loop structures are observed. The DNA-CNT adhesion energy (the absolute value of the DNA-CNT vdW energy) decreases for larger tube radius, while the DNA strain energy (backbone bond stretching, bending, and torsion) is found to be on the same level for all the tubes. Therefore, the final wrapping structure should be mainly driven by the DNA-CNT vdW interactions.

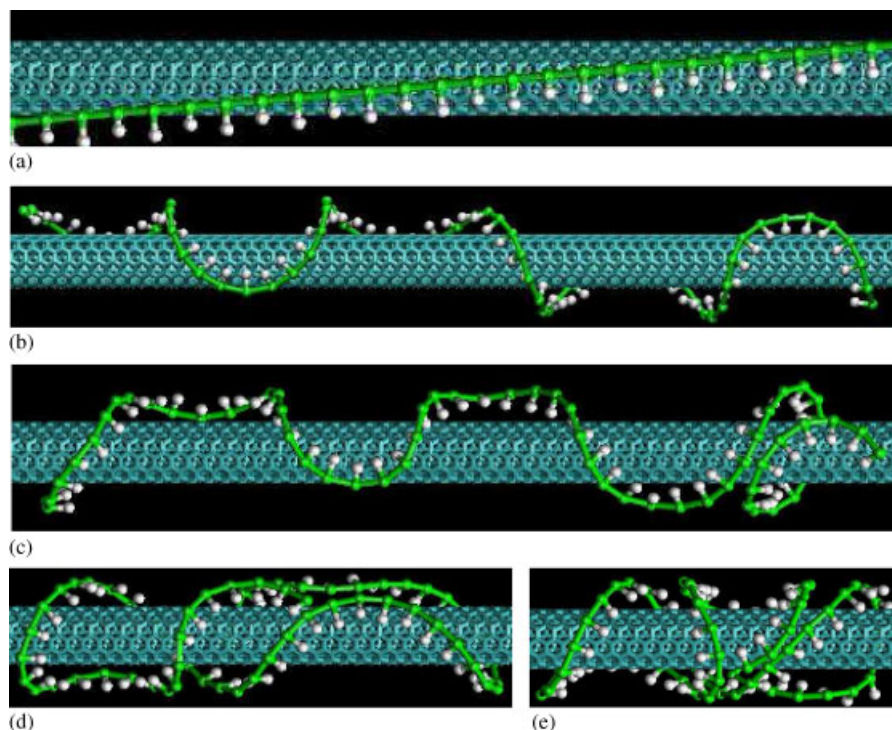


Figure 9. (Color Online) Other characteristic wrapping configurations formed by a 60-base-long ssDNA wrapping around a (6, 6) CNT with different initial configurations after 100 ns simulations. (a) A representative initial configuration, where the linear ssDNA forms an angle of $\vartheta = 15^\circ$ with the CNT axis; (b) U-shaped wrapping for $\vartheta = 0^\circ$; (c) U-shaped wrapping for $\vartheta = 30^\circ$; (d) self-contact loop for $\vartheta = 60^\circ$; and (e) random wrapping for $\vartheta = 90^\circ$.

4. CONCLUDING REMARKS

In summary, we have developed a coarse-grained model to simulate DNA-CNT interactions. The coarse-grained treatment involves representing each DNA nucleotide by only two interaction sites and constructing the interaction potentials between the interaction sites and the carbon atoms through all-atom MD simulations. Solvent effect is implicitly taken into account by Langevin dynamics. With these treatments, the number of degrees of freedom of the DNA-CNT hybrids is dramatically reduced. Using this coarse-grained method, we have performed a series of simulations to explore the adhesion, encapsulation, and wrapping process of DNA-CNT complexes formed by self-assembly in aqueous environment. The results agree well with all-atom MD simulations and experimental results in several aspects. The adhesion energy of DNA bases at the CNT exterior surface increases as the tube radius increases and decreases at the interior surface, with higher values for purines and lower values for pyrimidines. The encapsulation process of DNA into SWCNT depends on the tube size and initial configuration, and the insertion speed increases nearly linearly with the simulation temperature. For DNA wrapping around SWCNTs, the final wrapping configuration of DNA strand is due to the interplay between the nonbonding interaction

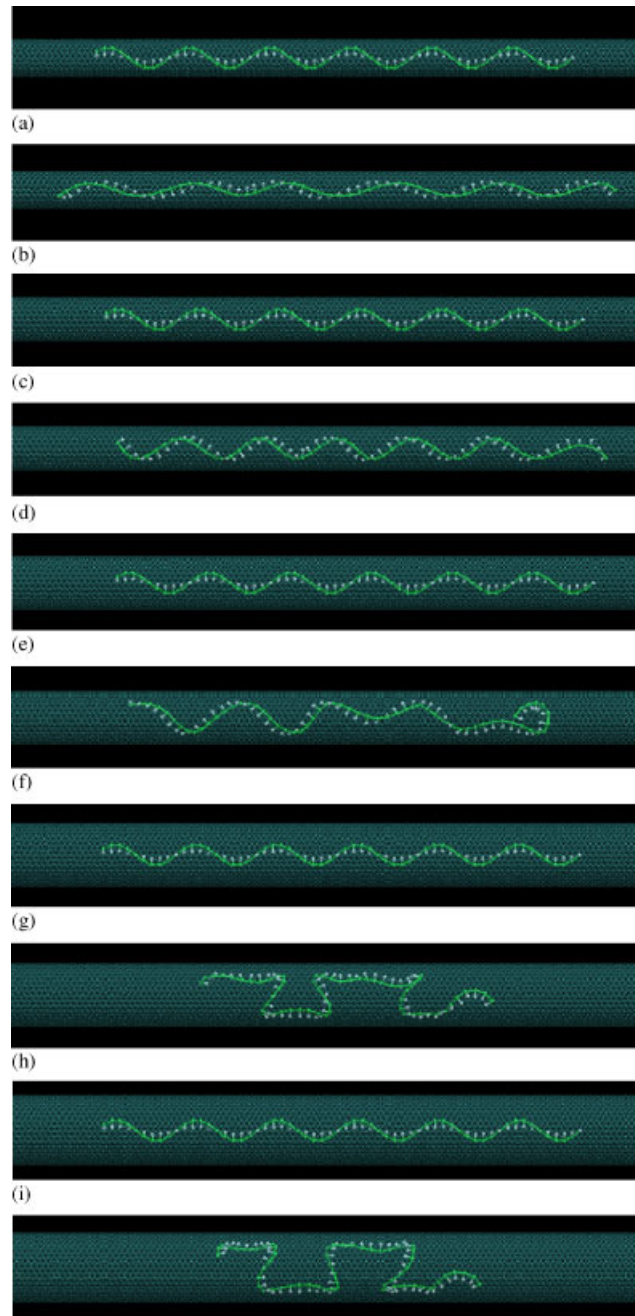


Figure 10. (Color Online) Wrapping configurations formed by a 60-base-long ssDNA wrapping around a SWCNT with different radii. (a)–(b), (c)–(d), (e)–(f), (g)–(h), and (i)–(j) are the initial and final configurations after 100 ns simulations for (10, 10), (12, 12), (15, 15), (18, 18), and (20, 20) CNTs, respectively.

and the relaxation of backbone bending and torsion. Depending on the initial configuration, a wide range of wrapping conformations are observed, including helices, U-shaped loops, and other more disordered structures. The coarse-grained model facilitates long-time simulations and provides useful guidelines of long DNA strand interaction with CNTs during self-assembling processes, or adhesion, peeling, and pushing, as were done in single-molecule experimental studies [2–4, 7–9].

ACKNOWLEDGEMENTS

We gratefully acknowledge the support from the National Science Foundation (NSF) grant under Awards No. 0600661(0826841) and 0600642 (Clark V. Cooper, program manager). We also thank Dr X. H. Shi and Dr R. R. Johnson for helpful discussions.

REFERENCES

1. Sarikaya M, Tamerler C, Jen AKY, Schulten K, Baneyx F. Molecular biomimetics: nanotechnology through biology. *Nature Materials* 2003; **2**(9):577–585.
2. Bashir R. DNA-mediated artificial nanobiostructures: state of the art and future directions. *Superlattices and Microstructures* 2001; **29**(1):1–16.
3. Zheng M, Jagota A, Strano MS, Santos AP, Barone P, Chou SG, Diner BA, Dresselhaus MS, McLean RS, Onoa GB, Samsonidze GG, Semke ED, Usrey M, Walls DJ. Structure-based carbon nanotube sorting by sequence-dependent DNA assembly. *Science* 2003; **302**(5650):1545–1548.
4. Zheng M, Jagota A, Semke ED, Diner BA, McLean RS, Lustig SR, Richardson RE, Tassi NG. DNA-assisted dispersion and separation of carbon nanotubes. *Nature Materials* 2003; **2**(5):338–342.
5. Gao H, Kong Y, Cui D, Ozkan CS. Spontaneous insertion of DNA oligonucleotides into carbon nanotubes. *Nano Letters* 2003; **3**(4):471–473.
6. Johnson RR, Johnson ATC, Klein ML. Probing the structure of DNA-carbon nanotube hybrids with molecular dynamics. *Nano Letters* 2008; **8**(1):69–75.
7. Staii C, Johnson AT. DNA-decorated carbon nanotubes for chemical sensing. *Nano Letters* 2005; **5**(9):1774–1778.
8. Tang XW, Bansaruntip S, Nakayama N, Yenilmez E, Chang YL, Wang Q. Carbon nanotube DNA sensor and sensing mechanism. *Nano Letters* 2006; **6**(8):1632–1636.
9. Meng S, Maragakis P, Papaloukas C, Kaxiras E. DNA nucleoside interaction and identification with carbon nanotubes. *Nano Letters* 2007; **7**(1):45–50.
10. Nelson DL, Cox MM. *Lehninger Principles of Biochemistry* (3rd edn). W.H. Freeman & Company: New York, 2000.
11. Iijima S. Helical microtubules of graphitic carbon. *Nature* 1991; **354**(6348):56–58.
12. Chen RJ, Bangsaruntip S, Drouvalakis KA, Kam NWS, Shim M, Li YM, Kim W, Utz PJ, Dai HJ. Noncovalent functionalization of carbon nanotubes for highly specific electronic biosensors. *Proceedings of the National Academy of Sciences of the United States of America* 2003; **100**(9):4984–4989.
13. Wohlstadter JN, Wilbur JL, Sigal GB, Biebuyck HA, Billadeau MA, Dong LW, Fischer AB, Gudiband SR, Jamieson SH, Kenten JH, Leginus J, Leland JK, Massey RJ, Wohlstadter SJ. Carbon nanotube-based biosensor. *Advanced Materials* 2003; **15**(14):1184–1187.
14. Clendenin J, Tung S, Budraa N, Mai J. Simulation of thin metal film bonding for MEMS applications inside a microwave cavity. *International Journal of Nonlinear Sciences and Numerical Simulation* 2002; **3**(3–4):779–784.
15. Keren K, Berman RS, Buchstab E, Sivan U, Braun E. DNA-templated carbon nanotube field-effect transistor. *Science* 2003; **302**(5649):1380–1382.
16. Liu WK, Karpov EG, Zhang S, Park HS. An introduction to computational nanomechanics and materials. *Computer Methods in Applied Mechanics and Engineering* 2004; **193**:1529–1578.
17. Cheatham TE, Kollman PA. Molecular dynamics simulation of nucleic acids. *Annual Review of Physical Chemistry* 2000; **51**:435–471.
18. Gao HJ, Kong Y. Simulation of DNA-nanotube interactions. *Annual Review of Materials Research* 2004; **34**:123–150.
19. Drukker K, Wu GS, Schatz GC. Model simulations of DNA denaturation dynamics. *Nature* 2001; **414**:579–590.
20. Marko JF, Siggia ED. Statistical-mechanics of supercoiled DNA. *Physical Review E* 1995; **52**(3):2912–2938.

21. Bustamante C, Marko JF, Siggia ED, Smith S. Entropic elasticity of lambda-phage DNA. *Science* 1994; **265**(5178):1599–1600.
22. Huertas ML, Navarro S, Martinez MCL, delaTorre JG. Simulation of the conformation and dynamics of a double-helical model for DNA. *Biophysical Journal* 1997; **73**(6):3142–3153.
23. Knotts TA, Rathore N, Schwartz DC, de Pablo JJ. A coarse grain model for DNA. *Journal of Chemical Physics* 2007; **126**(8):084901.
24. Tepper HL, Voth GA. A coarse-grained model for double-helix molecules in solution: Spontaneous helix formation and equilibrium properties. *Journal of Chemical Physics* 2005; **122**(12):124906.
25. Arroyo M, Belytschko T. Finite crystal elasticity of carbon nanotubes based on the exponential Cauchy-Born rule. *Physical Review B* 2004; **69**(11):115415.
26. Arroyo M, Belytschko T. Finite element methods for the non-linear mechanics of crystalline sheets and nanotubes. *International Journal for Numerical Methods in Engineering* 2004; **59**(3):419–456.
27. Zhang SL, Mielke SL, Khare R, Troya D, Ruoff RS, Schatz GC, Belytschko T. Mechanics of defects in carbon nanotubes: atomistic and multiscale simulations. *Physical Review B* 2005; **71**(11):115403.
28. Zhang SL, Zhu T, Belytschko T. Atomistic multiscale analyses of brittle fracture in crystal lattices. *Physical Review B* 2007; **76**:094114.
29. Zou J, Huang X, Arroyo M, Zhang SL. Effective coarse-grained simulations of super-thick multi-walled carbon nanotubes under torsion. *Journal of Applied Physics* 2009; **105**(3):033516.
30. Zhang SL, Khare R, Lu Q, Belytschko T. A bridging domain and strain computation method for coupled atomistic-continuum modelling of solids. *International Journal for Numerical Methods in Engineering* 2007; **70**(8):913–933.
31. Cornell WD, Cieplak P, Bayly CI, Gould IR, Merz KM, Ferguson DM, Spellmeyer DC, Fox T, Caldwell JW, Kollman PA. A 2nd generation force-field for the simulation of proteins, nucleic-acids, and organic-molecules. *Journal of the American Chemical Society* 1995; **117**(19):5179–5197.
32. Walther JH, Jaffe R, Halicioglu T, Koumoutsakos P. Carbon nanotubes in water: structural characteristics and energetics. *Journal of Physical Chemistry B* 2001; **105**(41):9980–9987.
33. Jorgensen WL, Chandrasekhar J, Madura JD, Impey RW, Klein ML. Comparison of simple potential functions for simulating liquid water. *The Journal of Chemical Physics* 1983; **79**(2):926–935.
34. Berendsen HJC, van der Spoel D, van Drunen R. Gromacs—a message-passing parallel molecular-dynamics implementation. *Computer Physics Communications* 1995; **91**(1–3):43–56.
35. Lindahl E, Hess B, van der Spoel D. GROMACS 3.0: a package for molecular simulation and trajectory analysis. *Journal of Molecular Modeling* 2001; **7**(8):306–317.
36. Berendsen HJC, Postma JPM, van Gunsteren WF, DiNola A, Haak JR. Molecular dynamics with coupling to an external bath. *The Journal of Chemical Physics* 1984; **81**(8):3684–3690.
37. Essmann U, Perera L, Berkowitz ML, Darden T, Lee H, Pedersen LG. A smooth particle mesh Ewald method. *Journal of Chemical Physics* 1995; **103**(19):8577–8593.
38. Shi XH, Kong Y, Gao HJ. Coarse grained molecular dynamics and theoretical studies of carbon nanotubes entering cell membrane. *Acta Mechanica Sinica* 2008; **24**(2):161–169.
39. Gowtham S, Scheicher RH, Ahuja R, Pandey R, Karna SP. Physisorption of nucleobases on graphene: density-functional calculations. *Physical Review B* 2007; **76**(3):033401.
40. Meng S, Wang WL, Maragakis P, Kaxiras E. Determination of DNA-base orientation on carbon nanotubes through directional optical absorbance. *Nano Letters* 2007; **7**(8):2312–2316.
41. Sowerby SJ, Cohn CA, Heckl WM, Holm NG. Differential adsorption of nucleic acid bases: relevance to the origin of life. *Proceedings of the National Academy of Sciences of the United States of America* 2001; **98**(3):820–822.